Pajot, P. (1976) *Eur. J. Biochem. 63*, 263-269.
Penefsky, H. S. (1967) *J. Biol. Chem. 242*, 5789-5795.
Penefsky, H. S. (1977) *J. Biol. Chem. 252*, 2891-2899.
Penefsky, H. S., & Warner, R. C. (1965) *J. Biol. Chem. 240*, 4694-4702.
Penin, F., Deléage, G., Gagliardi, D., Roux, B., & Gautheron, D. C. (1990) *Biochemistry 29*, 9358-9364.
Petrone, G., Garboczi, D. N., & Pedersen, P. L. (1987) *Biochemistry 26*, 4016-4021.
Pevec, B., Fassold, E., Uwira, N., & Hess, B. (1984) *Eur. Bioenerg. Conf. 3*, 351-352.
Prasad, A. R. S., Nishimura, J. S., & Horowitz, P. M. (1983) *Biochemistry 22*, 4272-4275.
Robinson, N. C., Tye, R. W., Neurath, H., & Walsh, K. A. (1971) *Biochemistry 10*, 2743-2747.
Roux, B., Fellous, G., & Godinot, C. (1984) *Biochemistry 23*, 534-537.
Sasaki, T., Abrams, B., & Horecker, B. L. (1975) *Anal. Biochem. 65*, 396-404.
Smith, P. K., Krohn, R. I., Hermanson, G. T., Mallia, A. K., Gartner, F. H., Provenzano, M. D., Fujimoto, E. K., Goeke, N. M., Olson, B. J., & Klenk, D. C. (1985) *Anal. Biochem. 150*, 76-85.
Takeda, K., Chen, W. J., Saltzgaber, J., & Douglas, M. G. (1986) *J. Biol. Chem. 261*, 15126-15133.
Tiedge, H., Lücken, U., Weber, J., & Schäfer, G. (1982) *Eur. J. Biochem. 127*, 291-299.
Tonomura, Y., Sekiya, K., & Imamura, K. (1962) *J. Biol. Chem. 237*, 3110-3115.
Vignais, P. V., & Lunardi, J. (1985) *Annu. Rev. Biochem. 54*, 977-1014.
Walker, J. E., Fearnley, I. M., Gay, N. J., Gibson, B. W., Northrop, F. D., Powell, S. J., Runswick, M. J., Saraste, M., & Tybulewicz, V. L. J. (1985) *J. Mol. Biol. 184*, 677-701.
Wang, J. H. (1988) *J. Bioenerg. Biomembr. 20*, 407-422.
Ysern, X., Amzel, L. M., & Pedersen, P. L. (1988) *J. Bioenerg. Biomembr. 20*, 423-450.

Structural Features of an Exocyclic Adduct Positioned opposite an Abasic Site in a DNA Duplex†

Michael Kouchakdjian,‡ Moises Eisenberg,§ Francis Johnson,§ Arthur P. Grollman,*,§ and Dinshaw J. Patel*,‡

Department of Biochemistry and Molecular Biophysics, College of Physicians and Surgeons, Columbia University, New York, New York 10032, and Department of Pharmacological Sciences, State University of New York at Stony Brook, Stony Brook, New York 11794

Received November 8, 1990; Revised Manuscript Received December 17, 1990

ABSTRACT: Structural studies have been extended to dual lesions where an exocyclic adduct is positioned opposite an abasic site in the center of a DNA oligomer duplex. NMR and energy minimization studies were performed on the 1,N^2-propanodeoxyguanosine exocyclic adduct (X) positioned opposite a tetrahydrofuran abasic site (F) with the dual lesions located in the center of the (C1-A2-T3-G4-*X5*-G6-T7-A8-C9)·(G10-T11-A12-C13-*F14*-C15-A16-T17-G18) X·F 9-mer duplex. Two-dimensional NMR experiments establish that the X·F 9-mer helix is right-handed with Watson–Crick A·T and G·C base pairing on either side of the lesion site. NOEs are detected from the methylene protons of the exocyclic ring of X5 to the imino protons of G4·C15 and G6·C13 which flank the lesion site, as well as to the H1′ and H1″ protons of the cross strand F14 tetrahydrofuran moiety. These NMR results establish that the exocyclic adduct X5 is positioned between flanking G4·C15 and G6·C13 base pairs and directed toward the abasic lesion F14 on the partner strand. These studies establish that the exocyclic ring of the 1,N^2-propanodeoxyguanosine adduct fits into the cavity generated by the abasic site.

Basu and Essigmann (1988), Harris et al. (1988), Singer and Grunberger (1983), and Singer and Bartsch (1986) have reviewed the structural and biological consequences of DNA-damaging agents. Our laboratories have approached this problem through NMR structural studies on site-specifically modified lesions in DNA oligomer duplexes. Early efforts were focused on O^6alkG lesions (Patel et al., 1986a–c; Kalnik et al., 1989b,c), O^4alkT lesions (Kalnik et al., 1988b,c), abasic sites (Kalnik et al., 1988a, 1989a), and exocyclic adducts (Kouchakdjian et al., 1989, 1990). These studies, along with contributions on abasic sites by others (Pochet et al., 1986; Raap et al., 1987; Cuniasse et al., 1987, 1989), provide insights into the conformation and pairing alignments at the lesion site and the interplay between hydrogen-bonding and hydrophobic interactions modulated by the pH of the solution (Kouchakdjian et al., 1990; Norman et al., 1989). Structural studies of DNA lesions in solution were undertaken within the same DNA sequence context as biological studies conducted in parallel in an attempt to understand the molecular basis of chemical mutagenesis and carcinogenesis.

NMR has been used to characterize structural features of modified DNA duplexes containing stable abasic sites (Kalnik et al., 1988, 1989a) and stable exocyclic adducts (Kouchakdjian et al., 1989, 1990). Oligonucleotides containing abasic sites have been shown to misincorporate dNTP's in reactions catalyzed by DNA polymerases (Takeshita et al., 1987). By determining the structural and biological properties of such lesions, we hope to understand the molecular basis of

†This research was supported by NIH Grants CA-46533 (abasic sites) and CA-49982 (exocyclic adducts) to D.J.P. and NIH Grants CA-17395 and CA-47995 to A.P.G.
‡Columbia University.
§State University of New York at Stony Brook.

0006-2960/91/0430-3262$02.50/0

the resulting mutagenic events.

Abasic sites in DNA arise under physiological conditions by spontaneous hydrolysis of the N-glycosidic bond (Lindahl & Nyberg, 1972; Loeb, 1985) or by the action of *N*-glycosylases on abnormal bases (Lindahl, 1982; Weiss & Grossman, 1987). The cyclic hemiacetal form of the 2-deoxyribose abasic site is unstable; in our studies we used the stable 3-hydroxy-2-(hydroxymethyl)tetrahydrofuran analogue **1** (Millican et al., 1984; Takeshita et al., 1987; Kalnik et al., 1988; Vesnaver et al., 1989).

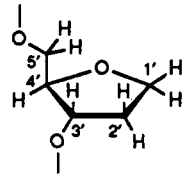

1

Exocyclic adducts can be generated by the reaction of bifunctional compounds with purine and pyrimidine bases (Shapiro, 1969). Resulting cyclic derivatives interfere with base pairing; such structures may play an important role in chemical mutagenesis. These collaborative structural and mutagenesis studies have focused on the model exocyclic 1,N^2-propanodeoxyguanosine adduct **2** (Marinelli et al., 1989; Kouchakdjian et al., 1989, 1990), a chemically stable analogue of the adduct generated by addition of acrolein to deoxyguanosine (Chung et al., 1984).

2

The present paper addresses structural questions related to opposing lesions in a DNA oligomer duplex. Our initial efforts focused on an exocyclic adduct positioned opposite an abasic site in the center of a DNA helix. The cyclic abasic site (F) **1** was incorporated in the sequence context d(G10-T11-A12-C13-*F14*-C15-A16-T17-G18) studied previously (Kalnik et al., 1988a), and the 1,N^2-propanodeoxyguanosine exocyclic adduct (X) **2** was also incorporated in the sequence context d(C1-A2-T3-G4-*X5*-G6-T7-A8-C9), also studied by NMR (Kouchakdjian et al., 1989, 1990). The two complementary strands generated a duplex **3** which contains an X5·F14 dual lesion site in the center of the 9-mer helix. Our goal was to

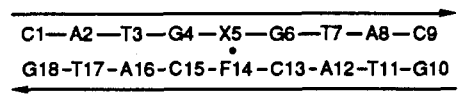

3

characterize whether the extra ring of the exocyclic adduct could be accommodated within the cavity generated by the abasic site on the partner strand and to deduce structural features of this potential alignment of opposing lesions. The importance of multiple lesions to mutagenesis remains to be established.

Experimental Procedures

Oligonucleotide Synthesis. The preparation of oligonucleotides containing a modified tetrahydrofuran abasic site **1** (designated F) (Takeshita et al., 1987; Kalnik et al., 1988a) and the exocyclic 1,N^2-(1,3-propano)-2′-deoxyguanosine adduct **2** (designated X) (Kouchakdjian et al., 1989; Marinelli et al., 1989) has been described previously.

Sample Preparation. A 1:1 stoichiometric mixture of the d(C-A-T-G-*X*-G-T-A-C) exocyclic adduct containing strand and the d(G-T-A-C-*F*-C-A-T-G) abasic site containing strand in the X·F 9-mer duplex **3** was achieved by monitoring the base proton resonances during strand addition at 50 °C. NMR experiments were performed on 200 A_{260} units of the X·F 9-mer duplex dissolved in 0.4 mL of 0.1 M NaCl, 10 mM phosphate, and 1 mM EDTA in either 100% D_2O or 90% H_2O/10% D_2O (v/v). The pH values recorded in D_2O are uncorrected pH meter readings.

NMR Experiments. One- and two-dimensional proton data sets on the X·F 9-mer duplex were collected on a Bruker AM 500 spectrometer. Proton chemical shifts are referenced relative to sodium 3-(trimethylsilyl)propionate-*2,2,3,3-d*$_4$ (TSP). Phosphorus spectra were recorded on an AM 300 spectrometer and are referenced relative to internal trimethyl phosphate (TMP).

Two-dimensional phase-sensitive NOESY spectra of the X·F 9-mer duplex in H_2O solution were collected by using a 120-ms mixing time and a 1.0-s. repetition delay. A jump and return ($90°_y$, τ, $90°_{-y}$) solvent suppression pulse (Plateau & Gueron, 1982) was used for detection, while the preparation and mixing pulses used 70° hard pulses. The carrier frequency was centered on the H_2O signal, and the waiting time was optimized for even excitation of the imino and aromatic protons. Each of the 256 t_1 increments collected consisted of 1024 complex data points acquired with 256 scans over a spectral width of 10000 Hz in the t_2 dimension. The free induction decays were apodized with a 90°-shifted sine bell function zeroed at the 1024th point in the t_2 dimension and at the 256th point in the t_1 dimension. Each dimension was base line corrected with a fifth-order polynomial base-line fitting routine following Fourier transformation.

Two-dimensional phase-sensitive NOESY spectra were collected on the X·F 9-mer duplex in D_2O buffer with a repetition delay of 1.5 s, a spectral width of 5000 Hz, and mixing times of 50 and 250 ms. The carrier frequency was positioned on the residual HOD resonance, and this resonance was presaturated by using the decoupler channel. The data sets were collected with 256 t_1 increments by using 1024 complex data points in the t_2 dimension and 32 scans per t_1 increment. The NOESY data sets were apodized with a 90°-shifted sine bell function zeroed at the 1024th point in the t_2 dimension and at the 256th data point in the t_1 dimension prior to Fourier transformation.

Processing of two-dimensional data sets were performed on a microVAX-II computer using FTNMR software. Two-dimensional data sets were processed according to the t_1 noise reduction routine of Otting et al. (1985).

Energy Minimization. The starting structure for the X·F 9-mer duplex was built by using standard B-DNA nucleotides with the X5·F14 lesion site generated from a G5·C14 base pair. The propano bridge was coupled to the deoxyguanosine base to generate the 1,N^2-propanodeoxyguanosine exocyclic adduct. The tetrahydrofuran moiety was prepared by replacing the deoxycytidine base by a hydrogen atom at the C1 position of the deoxyribose. The glycosidic torsion angle of X5 was set to the anti orientation for the starting model as established by NMR.

The starting structure was energy minimized by using the program XPLOR (Prof. A. Brunger, Yale University) with 5000 steps using the conjugate gradient protocol with 141 NOE determined distances applied as square-well potential constraints. These distance constraints were estimated from the

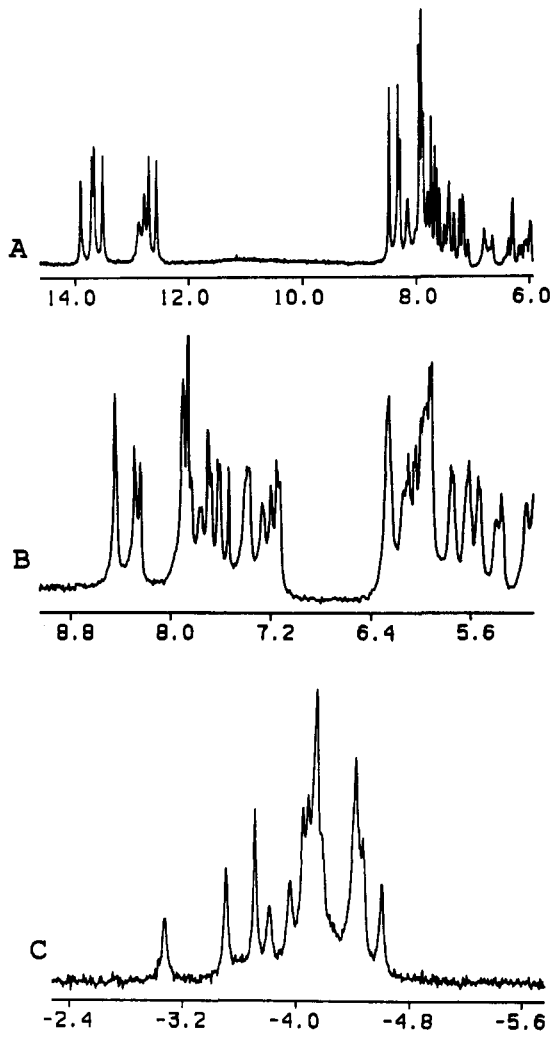

FIGURE 1: NMR spectra of the X·F 9-mer duplex in 0.1 M NaCl and 10 mM phosphate, aqueous solution, pH 7.3 at 10 °C. (A) Exchangeable 500-MHz proton spectra (6.0–14.0 ppm) in H_2O buffer. (B) Nonexchangeable 500-MHz proton spectra (5.0–9.0 ppm) in D_2O buffer. (C) Proton-decoupled 121-MHz phosphorus spectra (−2.4 to −5.6 ppm).

cross peak volume integrals in the NOESY spectra of the X·F 9-mer duplex in D_2O at mixing times of 50 and 250 ms. The deviations in the lower bounds ranged from 0.6 to 0.9 Å, and the deviations in the upper bounds ranged from 0.8 to 1.0 Å for distances extracted from the 50-ms mixing time NOESY data set with the tighter bounds associated with the shorter distances. The deviations in the lower and upper bounds ranged from 1.0 to 1.2 Å for distances extracted from the 250-ms mixing time NOESY data set with the tightness of the bounds again dependent on distance. We did not estimate distances for overlapping cross peaks in the NOESY spectra of the X·F 9-mer duplex.

Watson–Crick base pairs were maintained during the minimization by applying square-well potential constraints. Electrostatic potential energy terms were based on a fully charged set of partial charges (−1 per residue) with a dielectric constant of 80.

RESULTS

Exchangeable Protons. The exchangeable proton spectrum (6.0–14.5 ppm) of the X·F 9-mer duplex, pH 7.3 at 10 °C in H_2O buffer, is shown in Figure 1A. The imino protons of thymidine and guanosine are well resolved and resonate at chemical shifts between 12.0 and 14.0 ppm while the exchangeable amino protons and nonexchangeable base protons resonate between 6.5 and 8.5 ppm. The observation of four resolved thymidine and four resolved guanosine imino protons allows us to monitor the presence of G·C and A·T base pairs in the nonanucleotide duplex.

Table I: Exchangeable Proton Chemical Shifts in the X·F 9-mer Duplex at 10 °C[a]

base pair	chemical shift (ppm)				
	T-H3	G-H1	C-H4b[b]	C-H4e[c]	A-H2
C1·G18		12.64	8.12	7.03	
A2·T17	13.65				7.84
T3·A16	13.85				7.82
G4·C15		12.64	8.27	7.45	
G6·C13		12.50	7.86	6.60	
T7·A12	13.46				7.52
A8·T11	13.61				7.60
C9·G10		12.71	8.08	6.73	

[a] 0.1 M NaCl and 10 mM phosphate, H_2O, pH 7.3. [b] Hydrogen-bonded cytidine amino proton. [c] Exposed cytidine amino proton.

The symmetrical contour plot (0–15 ppm) of the phase-sensitive NOESY spectrum (120-ms mixing time) of the X·F 9-mer duplex at pH 7.3, 10 °C in H_2O buffer, is presented in Figure 2A. Expanded regions of this spectrum featuring NOEs between adjacent imino protons (12.0–14.2 ppm) and between imino protons and exchangeable amino and nonexchangeable base protons (6.4–8.8 ppm) are displayed in Figure 3, panels A and B, respectively. Cross peaks can be monitored between thymidine imino and adenosine H2 protons in the A2·T17 (peak D, Figure 3B), T3·A16 (peak C, Figure 3B), T7·A12 (peak F, Figure 3B), and A8·T11 (peak E, Figure 3B) base pairs. NOEs are also detected for the base pairs immediately flanking the X·F dual lesion between the guanosine imino and the hydrogen-bonded and exposed cytidine amino protons in the G4·C15 (peaks H and I, Figure 3B) and G6·C13 (peaks J and K, Figure 3B) base pairs. Additional NOEs are detected between the imino protons of adjacent T3·A16 and G4·C15 (peak A, Figure 3A) and G6·C13 and T7·A12 (peak B, Figure 3A) base pairs.

The well-resolved guanosine imino protons of the G4·C15 (12.64 ppm) and the G6·C13 (12.50 ppm) base pairs which flank the exocyclic lesion site display a number of relatively weak NOEs to the CH_2 protons of the propano bridge of the adjacent exocyclic base (X5) (boxed region, Figure 2A). The imino proton of G4 shows NOEs to all resolved CH_2 protons of the exocyclic ring, whereas the G6 imino proton exhibits NOEs to only the CH_2 protons to highest field. These cross peaks are confirmed by one-dimensional NOE difference experiments (Figure S1; see supplementary material).

The chemical shifts of the imino and amino protons and the adenosine H2 protons in the X·F 9-mer duplex in H_2O buffer, pH 7.3 at 10 °C, are tabulated in Table I.

Nonexchangeable Protons. The nonexchangeable protons of the X·F 9-mer duplex (base and H1′ regions plotted in Figure 1B) can be assigned by recording two-dimensional proton NMR spectra in D_2O solution. A symmetrical contour plot (1.0–9.0 ppm) of the phase-sensitive NOESY spectrum (250-ms mixing time) of the X·F 9-mer duplex in D_2O buffer, pH 7.3 at 10 °C, is plotted in Figure 2B.

An expanded contour plot establishing distance connectivities between the base protons (7.0–8.6 ppm) and the sugar H1′ and cytidine H5 protons (5.2–6.4 ppm) in the X·F 9-mer duplex is shown in duplicate in Figure 4. The most intense cross peaks correspond to the short cytidine H5–H6 distance connectivities (designated by asterisks in Figure 4). Each purine H8 and pyrimidine H6 proton should exhibit NOEs

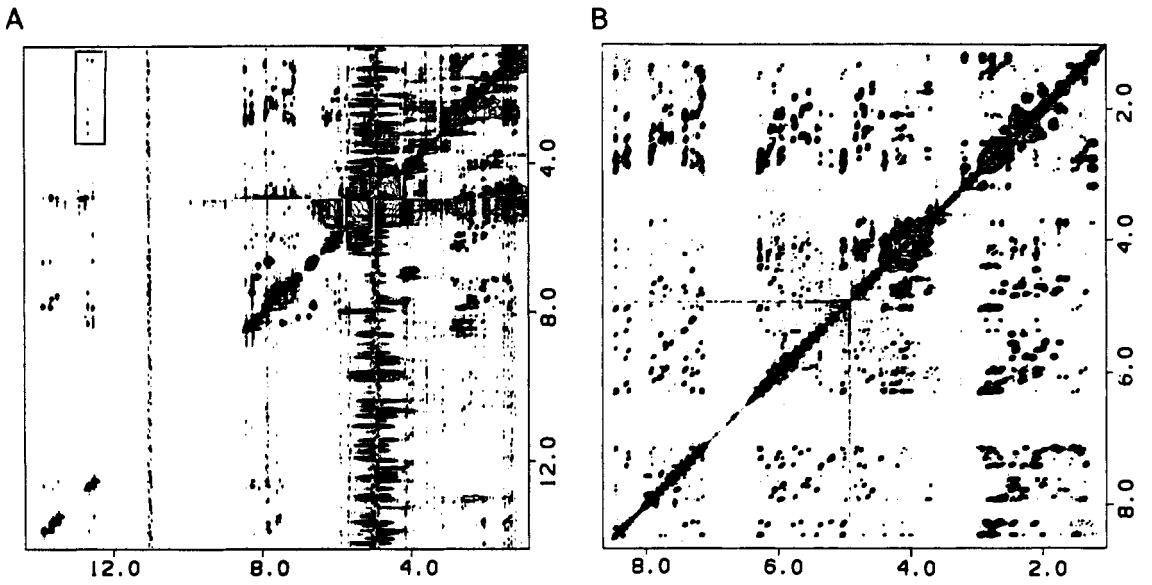

FIGURE 2: Phase-sensitive NOESY contour plots of the X·F 9-mer duplex in 0.1 M NaCl and 10 mM phosphate, aqueous solution, pH 7.3 at 10 °C. (A) Symmetrical 1.0–14.0 ppm region in H_2O buffer recorded at a mixing time of 120 ms. Boxed region is discussed in the text. (B) Symmetrical 1.0–9.0 ppm region in D_2O buffer recorded at a mixing time of 250 ms.

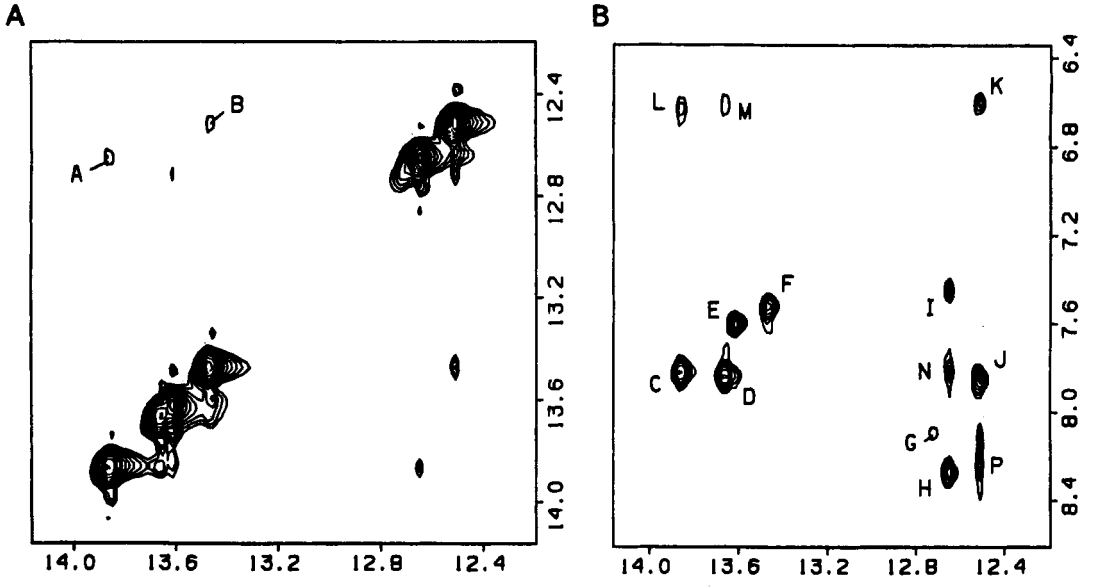

FIGURE 3: Expanded phase-sensitive NOESY (120-ms mixing time) contour plots of the X·F 9-mer duplex in H_2O buffer, pH 7.3 at 10 °C. (A) Cross peaks establishing connectivities between imino protons in the symmetrical 12.0–14.4 ppm spectral range. (B) Cross peaks between the imino protons (12.0–14.4 ppm) and the base and amino protons (6.4–8.6 ppm). Labeled cross peaks are discussed in the text.

to its own and 5′-flanking sugar H1′ protons in right-handed DNA (Hare et al., 1983). The deoxynucleotide chain can readily be traced from C1 to G4 and from G6 to C9 in the exocyclic adduct-containing strand (Figure 4A), and from G10 to C13 and C15 to G18 in the strand that contains the abasic site (Figure 4B). The interruption in the chain tracing for the exocyclic-modified strand reflects the absence of detectable NOEs between the H8 of X5 and its own sugar H1′ proton and between the H8 of G6 and the H1′ proton of X5 its 5′-flanking neighbor (Figure 4A). On the abasic site containing strand, the interruption of the chain tracing reflects the absence of the base at F14.

NOE cross peaks are detected between purine H8 and pyrimidine H5/CH_3 protons on adjacent bases for purine(3′–5′)pyrimidine steps for A2-T3, G6-T7, A8-C9, G10-T11, A12-C13, and A16-T17 steps, and the directionalities of these NOES are characteristic of the handedness of the helix.

The 250- and 50-ms mixing time expanded NOESY stacked plots between the base protons and the sugar H1′ protons of the X·F 9-mer duplex at pH 7.3 are plotted in Figure S2, panels A and B, respectively (see supplementary material). The intensities of the NOES from the base to their own sugar H1′ protons are weak relative to the intensitives of the NOEs between the cytidine H5 to H6 protons in the 50-ms NOESY data set (Figure S2B).

Expanded NOESY contour plots establishing distance connectivities between the sugar H2′,2″ protons (1.2–3.0 ppm) and the base protons (7.0 and 8.6 ppm) and the sugar H1′ protons (5.2–6.4 ppm) in the X·F 9-mer duplex are displayed in Figure 5, panels A and B, respectively. All expected cross peaks in these two expanded region are present with the exception of the NOEs between the sugar H1′ proton and its own sugar H2′,2″ protons for X5 (Figure 5B). Weak NOE cross peaks are detected between the H2′,2″ protons of F14 and the H6 (boxed peaks, Figure 5A) and H5 protons (boxed peaks, Figure 5B) of the flanking C15 residue. Additionally, there are no NOEs detected between any of the nonexchangeable base or sugar H1′ protons of the unmodified nucleotides and

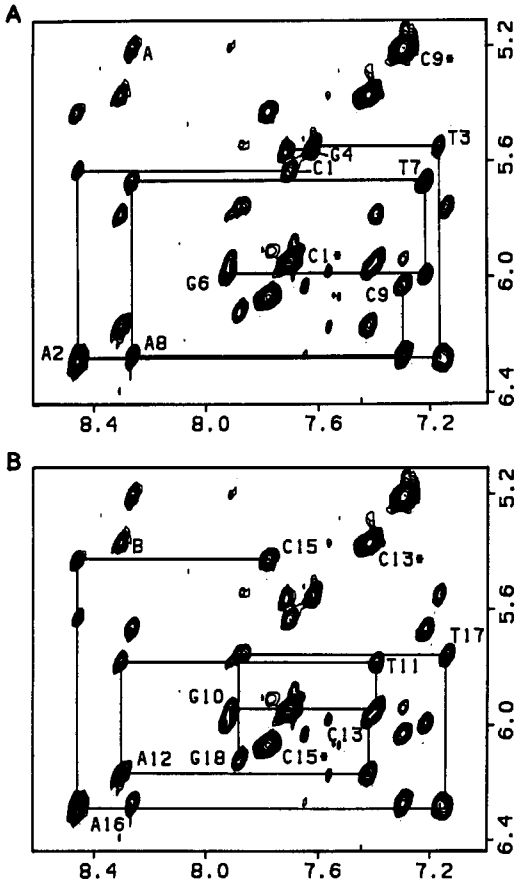

FIGURE 4: Expanded contour plots of the phase-sensitive NOESY spectrum (mixing time 250 ms) of the X·F 9-mer duplex in D_2O buffer, pH 7.3 at 10 °C. Distance connectivities are shown between the base protons (7.0–8.6 ppm) and the sugar H1′ and cytidine H5 protons (5.1–6.4 ppm). (A) Tracing of the oligonucleotide chain from C1 to C9. (B) Chain tracing from G10 to G18. The tracing follows connectivities between adjacent base protons through their own and 5′-flanking sugar H1′ protons. The deoxycytidine H6–H5 cross peaks are designated by asterisks. Cross peaks A and B are assigned as follows: (A) A8(H8) to C9(H5); (B) A12(H8) to C13(H5).

Table II: Nonexchangeable Proton Chemical Shifts in the X·F 9-mer Duplex at 10 °C[a]

	chemical shift (ppm)						
base	H8	H2	H6	H5/CH_3	H1′	H2′, H2″	H3′
C1			7.70	5.94	5.63	2.01, 2.42	4.72
A2	8.46	7.88			6.28	2.78, 2.93	5.03
T3			7.16	1.48	5.55	1.76, 1.98	4.76
G4	7.62				5.56	2.40, 2.49	
X5	7.71					2.43, 2.48	
G6	7.92				5.99	2.72, 2.82	5.00
T7			7.21	1.43	5.67	2.10, 2.43	4.84
A8	8.26	7.64			6.27	2.67, 2.87	5.01
C9			7.30	5.21	6.03	2.09, 2.13	
G10	7.91				5.94	2.63, 2.76	4.78
T11			7.39	1.35	5.78	2.15, 2.47	
A12	8.30	7.56			6.16	2.71, 2.84	5.03
C13			7.42	5.37	5.97	2.09, 2.32	4.71
F14					3.75, 3.75	1.65, 1.76	4.61
C15			7.78	6.06	5.43	2.31, 2.48	4.59
A16	8.46	7.86			6.29	2.80, 2.95	5.05
T17			7.14	1.55	5.76	1.83, 2.27	4.82
G18	7.88				6.12	2.33, 2.59	4.66

[a] 0.1 M NaCl and 10 mM phosphate, D_2O, pH 7.3.

the methylene protons of the propano bridge of the exocyclic adduct (chemical shifts between 1.0 and 3.5 ppm) (Figure 5).

An expanded NOESY contour plot of the symmetrical 1.2–4.8 ppm region of the X·F 9-mer duplex is plotted in Figure 6. This region displays NOEs among the CH_2 protons

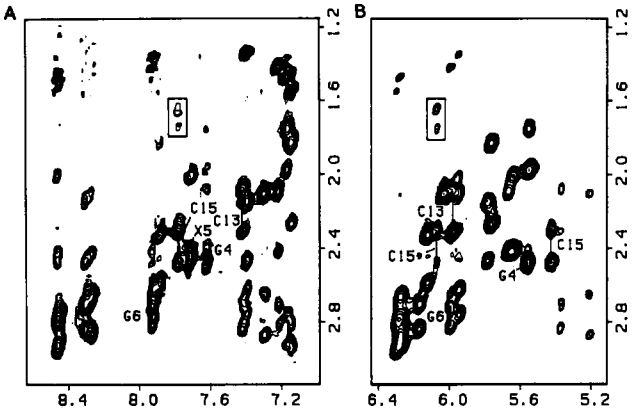

FIGURE 5: Expanded contour plots of the phase-sensitive NOESY spectrum (mixing time 250 ms) of the X·F 9-mer duplex in D_2O buffer, pH 7.3 at 10 °C. (A) NOE cross peaks establishing distance connectivities between the base protons (7.0–8.6 ppm) and the sugar H2′,2″ and exocyclic CH_2 protons (1.2–3.2 ppm). The symbols label NOEs between base protons and their own sugar H2′,2″ protons in the (G4-X5-G6)·(C13-F14-C15) segment. The boxed peaks are discussed in the text. (B) NOE cross peaks establishing distance connectivities between the sugar H1′ protons (5.2–6.4 ppm) and the sugar H2′,2″ and exocyclic CH_2 protons (1.2–3.2 ppm). The symbols label NOEs between the sugar H1′ and their own sugar H2′,2″ protons in the (G4-X5-G6)·(C13-F14-C15) segment. The boxed peaks are discussed in the text.

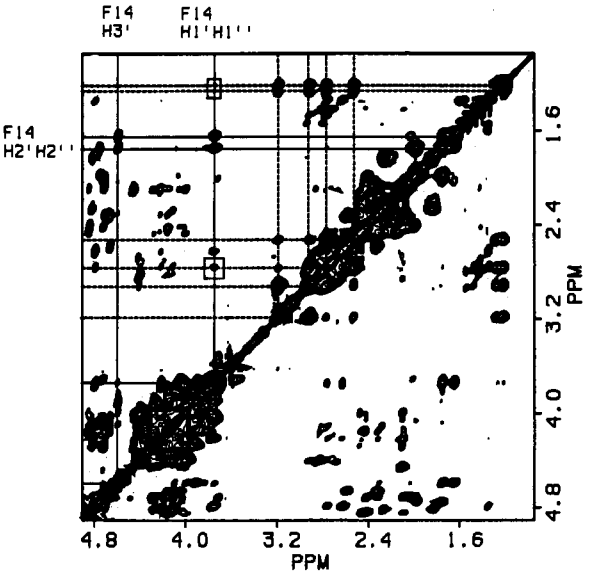

FIGURE 6: Expanded contour plot of the phase-sensitive NOESY spectrum (mixing time 250 ms) of the X·F 9-mer duplex in D_2O buffer, pH 7.3 at 10 °C. Plot shows the symmetrical 1.0–4.8 ppm region that includes sugar H2′,2″ protons and exocyclic CH_2 protons. Solid lines designate H1′,1″ (overlapping resonances), H2′,2″, and H3′ protons of F14. Dashed lines designate exocyclic CH_2 resonances. Boxed cross peaks are discussed in the text.

of the propano bridge of the exocyclic adduct (central CH_2 protons resonate at 1.22 and 1.28 ppm while flanking CH_2 proton pairs resonate at 2.54 and 2.77 ppm, and at 2.92 and 3.19 ppm for the flanking methylene proton pairs) (dashed lines, Figure 6) and also NOEs between the sugar proton of the F14 abasic site (H1′,1″ protons have the same chemical shift and resonate at 3.75 ppm, H2′,2″ protons resonate at 1.65 and 1.76 ppm, and the sugar H3′ proton resonates at 4.61 ppm) (solid lines, Figure 6). We detect weak cross strand NOE cross peaks between the H1′,1″ protons of F14 and both of the central CH_2 protons (1.22 and 1.28 ppm) and one of the flanking CH_2 protons (2.77 ppm) of X5 (boxed peaks, Figure 6) in the X·F 9-mer duplex.

Table III: Proton Chemical Shifts of Exocyclic CH_2 Protons in the X·F 9-mer Duplex, pH 7.3

	chemical shift (ppm)
central CH_2	1.22, 1.28
flanking CH_2	2.54, 2.77 and 2.92, 3.19

Table IV: Proton–Proton Distance Constraints in the (G4-X5-G6)·(C13-F14-C15) Segment of the X·F 9-mer Duplex

	intraresidue constraints on same strand (Å)				
	H6/H8–H1′	H6/H8–H2′	H6/H8–H2″	H1′–H2′	H1′–H2″
G4	2.8–5.2[d]	*a*	*a*	*a*	*a*
X5	*b*	*a*	*a*	*b*	*b*
G6	2.8–5.2[d]	*a*	2.7–4.6[c]	3.0–5.2[d]	2.2–3.9[c]
C13	2.8–5.2[d]	2.0–3.6[c]	3.0–4.9[c]	*a*	3.0–5.2[d]
F14				2.5–4.1[c]	2.5–4.1[c]
C15	2.8–5.2[d]	2.0–3.6[c]	3.3–5.0[c]	3.0–5.2[d]	3.0–5.2[d]

	interresidue constraints on same strand (Å)			
	H1′–H6/H8	H2′–H6/H8	H6/H8–H6/H8	H6/H8–H5/CH_3
T3-G4	2.8–5.2[d]	3.4–5.6[d]	3.4–5.6[d]	
G4-X5	2.8–5.2[d]	*a*	*b*	
X5-G6	*b*	3.4–5.6[d]	*b*	
G6-T7	2.8–5.2[d]	2.8–5.2[d]	3.3–5.5[d]	2.4–4.2[c]
A12-C13	2.8–5.2[d]	2.8–5.2[d]	3.3–5.5[d]	3.1–5.3[d]
C13-F14				
F14-C15	*b*	3.4–5.6[d]		
C15-A16	2.8–5.2[d]	2.8–5.2[d]	3.3–5.5[d]	

interresidue constraints on partner strands (Å)	
X5 CH_2 (1.22 ppm, 1.28 ppm)–F14 H1′	3.4–5.6[d]
X5 CH_2 (1.22 ppm, 1.28 ppm)–F14 H1″	3.4–5.6[d]

[a] Overlap. [b] Very weak or absent. [c] 50-ms NOESY data set. [d] 250-ms NOESY data set.

The base and sugar proton chemical shifts of the X·F 9-mer duplex, pH 7.3 at 10 °C, are listed in Table II. Exocyclic methylene proton chemical shifts are listed in Table III. These assignments are based on the analysis of all regions of the NOESY spectrum (Figure 2B) and have been confirmed by analysis of COSY data.

Phosphorus Spectrum. The proton-decoupled phosphorus spectrum of the X·F 9-mer duplex in D_2O buffer, pH 7.3 at 10 °C, is plotted in Figure 1C. The resolved internucleotide phosphates are dispersed between −3.0 and −4.8 ppm. Several phosphorus resonances fall outside the −4.0 to −4.5 ppm region characteristic of an unperturbed phosphodiester backbone. A contour plot of the proton-detected heteronuclear phosphorus–proton COSY spectrum of the X·F 9-mer duplex in D_2O solution, pH 7.3 at 10 °C, is plotted in Figure S3. The phosphorus resonances can be correlated with their three bond separated H3′ and H5′,5″ protons and their four bond separated H4′ protons (Figure S3). However, we are unable to make unambiguous phosphorus assignments in the absence of a complete set of H3′ proton assignments (Table II) for the X·F 9-mer duplex.

NMR Distance Constraints. The volume integrals of the NOE cross peaks for the X·F 9-mer were measured from the 50- and 250-ms mixing time NOESY data sets in D_2O buffer, pH 7.3 at 10 °C, and distance bounds established relative to cross peaks corresponding to the H6–H5 protons of cytidine (fixed 2.45-Å distance). These constraints, defined by conservative lower and upper bounds for the (G4-X5-G6)·(C13-F14-C15) segment of the X·F 9-mer duplex, are listed in Table IV. The distance bounds include base–sugar and sugar–sugar constraints within each nucleotide, base–base and base–sugar constraints between adjacent nucleotides, and cross strand constraints between the exocyclic CH_2 protons of X5 and the H1′,H1″ protons of F14 in the X·F 9-mer duplex.

Table V: Proton–Proton Distance in the (G4-X5-G6)·(C13-F14-C15) Segment of the X·F 9-mer Duplex from the Energy-Minimized Model

	intraresidue distances on the same strand (Å)				
	H6/H8–H1′	H6/H8–H2′	H6/H8–H2″	H1′–H2′	H1′–H2″
G4	3.9	2.4	3.6	3.1	2.5
X5	3.9	2.2	3.4	3.1	2.5
G6	3.9	2.4	3.6	3.1	2.5
C13	3.8	2.1	3.5	3.2	2.5
F14				3.1	2.5
C15	3.8	2.1	3.5	3.1	2.5

	interresidue distances on the same strand (Å)			
	H1′–H6/H8	H2′–H6/H8	H6/H8–H6/H8	H6/H8–H5/CH_3
T3-G4	3.2	4.2	4.8	
G4-X5	3.5	4.7	5.6	
X5-G6	3.0	4.0	4.6	
G6-T7	3.2	4.6	5.4	4.2
A12-C13	3.1	4.4	5.1	4.1
C13-F14				
F14-C15	2.6	4.2		
C15-A16	3.0	4.0	5.0	

interresidue distances on partner strands (Å)	
X5 CH_2 (1.22 ppm, 1.28 ppm)–F14 H1′	2.97, 3.19
X5 CH_2 (1.22 ppm, 1.28 ppm)–F14 H1″	2.29, 2.61

Energy Minimization Computations. The 141 experimental distance bounds for the X·F 9-mer duplex were incorporated as square-well potential constraints in the energy minimization algorithm of the XPLOR program. The starting structure of the helix was B-form, and the alignment of X5 was anti about the glycosidic bond. The minimization computation was guided by the distance bounds corresponding to the weak NOEs between the exocyclic CH_2 protons of X5 and the sugar H1′,H1″ protons of F14 at the X5·F14 lesion site. Following minimization, the final internal energy for the X·F 9-mer duplex was 105 kcal/mol.

A stereoview of the (G4-X5-G6)·(C13-F14-C15) segment normal to the helix axis emphasizes that the nonplanar exocyclic group of X5 is accommodated in the cavity created by the missing base at abasic site F14 without disruption of the flanking G4·C15 and C6·C13 base pairs (Figure 7A). A view down the helix axis of the X5·F14 site is shown in Figure 7B. Proton–proton distances for the (G4-X5-G6)·(C13-F14-C15) segment obtained for the energy-minimized conformation are listed in Table V.

Discussion

We have previously reported on NMR structural studies of the 1,N^2-propanodeoxyguanosine exocyclic adduct positioned opposite purine bases in the center of 9-mer DNA oligomer duplexes. These studies established the importance of pH in modulating the equilibrium between protonated X(syn)·A(anti) alignment stabilized by two hydrogen bonds at acidic pH (Kouchakdjian et al., 1989) and X(anti)·A(anti) alignment stabilized by hydrophobic interactions between partially stacked X and A bases at basic pH (Kouchakdjian et al., 1990). This paper reports studies of the 1,N^2-propanodeoxyguanosine exocyclic adduct positioned opposite a cyclic abasic site in the center of a 9-mer duplex **3** aimed at defining structural features at and adjacent to the double lesion site.

General Features of X·F 9-mer Duplex. Several general conclusions can be deduced following analysis of NOESY

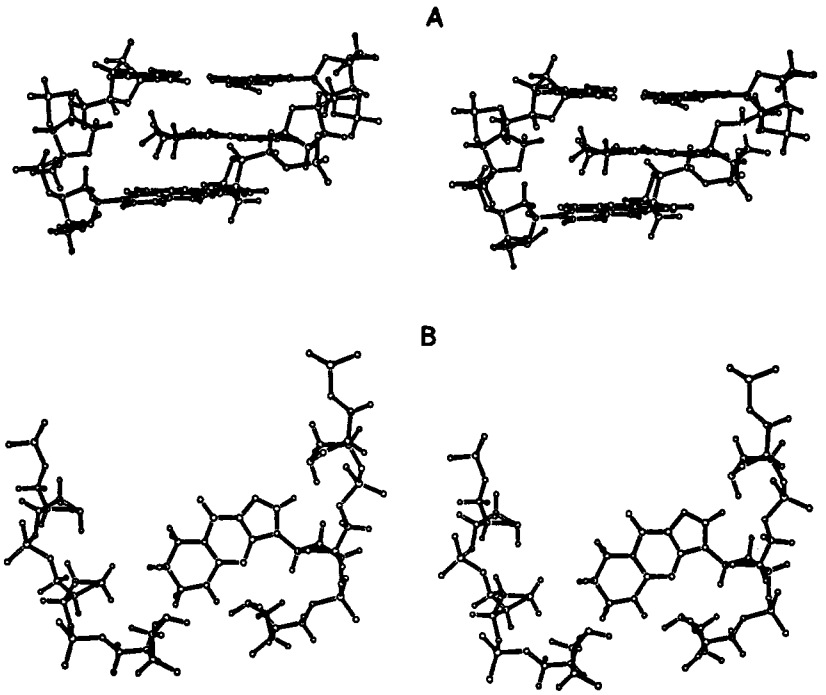

FIGURE 7: Stereopairs of (A) the (G4-X5-G6)·(C13-F14-C15) trinucleotide segment viewed normal to the helix axis and (B) the X5·F14 alignment viewed down the helix axis in the energy-minimized conformation of the X·F 9-mer duplex.

spectra of the X·F 9-mer duplex in H_2O and D_2O buffer solution. The observed NOEs between the thymidine imino and adenosine H2 protons for the A2·T17, T3·A16, T7·A12, and A8·T11 pairs and between the guanosine imino and the hydrogen-bonded and exposed cytidine amino protons for the G4·C15 and G6·C13 pairs readily establish that all nonterminal base pairs are of the Watson–Crick type in the X·F 9-mer duplex (Figure 3B). Furthermore, these results demonstrate that the X·F lesion site is flanked by intact G4·C15 and G6·C13 base pairs at low temperature (10 °C).

The handedness of the helix can be probed from the directionality of the base–sugar and base–base NOE connectivities between adjacent nucleotide units in the X·F 9-mer duplex. The observed NOEs between the base protons and their 5′-flanking sugar H1′, H2′,2″, and H3′ protons and between adjacent base protons in purine H8/pyrimidine H6-(3′–5′)pyrimidine H5/CH_3 steps are consistent with the X·F 9-mer adopting a right-handed helix in solution (Figures 4 and 5A).

A comparison of the NOE cross peak intensities of the base to its own sugar H1′ protons with those between the cytidine H6 and H5 protons at 50-ms mixing times (Figure S2B) establishes that all nucleotide glycosidic torsion angles are anti in the X·F 9-mer duplex.

X5 and F14 at the Lesion Site. The observed NOEs between several CH_2 protons on the nonplanar exocyclic ring of X5 and the exchangeable imino protons of G4 and G6 (boxed region, Figures 2A and S1) and the nonexchangeable H1′,H1″ protons of the F14 abasic site establish unequivocally that the exocyclic base, X5, is in the anti range and is positioned between adjacent G4·C15 and G6·C13 base pairs within the cavity generated by the abasic site. Our data further establish that the nonplanarity of the exocyclic ring does not prevent the insertion of the exocyclic adduct into the helix opposite the abasic site. The observed cross strand NOEs between X5 and F14 also suggest that the cyclic furan ring of the abasic site has not looped out of the helix in the X·F 9-mer duplex but rather retains its alignment within the helix. Recent studies have established that looped-out abasic sites exhibit NOEs between their H4′ proton and the sugar H2″ and H3′ protons of the 5′-flanking residue in a right-handed duplex (Cuniasse et al., 1989, 1990). We do not detect an NOE between the H4′ proton of F14 and the sugar H2″ proton of C13, which provides additional evidence that F14 is not looped out of the X·F 9-mer helix.

The NOE cross peak between the H8 of X5 and its own sugar H1′ proton is too weak to detect in the X·F 9-mer duplex (Figure 4A). Furthermore, the NOEs between the sugar H1′ proton of X5 and its own H2′,2″ protons have also not been detected (Figure 5B). These observations suggest that the line width of the sugar H1′ proton of X5 may be unusually broad, thus resulting in the absence of detectable NOEs from this sugar proton. The observed broadening of the H1′ proton of X5 could result from motion of the base about the helix axis with concomitant changes in the backbone angles which occur on the intermediate exchange time scale.

Distance Constraints and Energy Minimization. The interproton distances for the (G4-X5-G6)·(C13-F14-C15) segment of the energy-minimized conformation of the X·F 9-mer (Table V) are with some exceptions within the experimentally determined bounds (Table IV) deduced from the NOESY data sets. The wide range of the experimental distance bounds (Table IV) implies that the (G4-X5-G6)·(C13-F14-C15) conformation drawn in Figure 7 represents a low-resolution view of the X5·F14 lesion site and its flanking base pairs in solution. These limitations do not allow quantitative conclusions regarding helical parameters to be drawn at the current stage of the investigation. An additional reason for caution relates to the potential conformational flexibility in the pucker of the tetrahydrofuran F14 abasic site and the potential conformational variability in the glycosidic torsion of X5 within the anti range for the X5·F14 lesion site. Indeed, the cross strand distances between the CH_2 protons of X5 and the H1′ proton of F14 at the X5·F14 lesion site in the energy-minimized conformation are shorter (Table V) than the experimentally determined bounds (Table IV).

The bulky 1,N^2-propanodeoxyguanosine adduct fits readily into the abasic site cavity without disruption of flanking dG·dC

base pairs. This exocyclic adduct is not involved in hydrogen bonding and is stabilized primarily by hydrophobic stacking interactions.

Chemical Shifts for the (G4-X5-G6)·(C13-F14-C15) Segment. The proton chemical shifts in the trinucleotide segment centered about the X5·F14 dual-lesion site in the X·F 9-mer duplex (Tables I–III) can be compared with the corresponding parameters in the X5·A14 lesion site in the X·A 9-mer duplex at basic pH (Kouchakdjian et al., 1990) and the A5·F14 lesion site in the A·F 9-mer duplex (Kalnik et al., 1988a).

Five of the six exocyclic CH_2 protons exhibit similar chemical shifts in the X·F 9-mer duplex (1.22, 1.28, *2.54*, 2.77, 2.92, and 3.19 ppm) (Table III) and the X·A 9-mer duplex at basic pH (1.22, 1.22, *1.84*, 2.67, 2.86, and 3.06 ppm) (Kouchakdjian et al., 1990). The exocyclic ring of X5 is directed toward the interior of the helix in both duplexes, and its protons experience upfield ring current contributions from the flanking stacked bases.

Proton chemical shifts for the tetrahydrofuran F14 moiety in the X·F 9-mer duplex (H1′,1″ 3.75, 3.75 ppm, H2′,2″ 1.65, 1.76 ppm, and H3′ 4.61 ppm) (Table II) are similar to those reported for the A·F 9-mer duplex (H1′,1″ 3.87, 3.96 ppm, H2′,2″ 1.92, 1.92 ppm, and H3′ 4.61 ppm) (Kalnik et al., 1988a), possibly suggesting similar alignments of F14 in the two duplexes.

The H8 proton chemical shifts of the purine bases in the G4-X5-G6 segment in the X·F 9-mer duplex (G4 7.62 ppm, X5 7.71 ppm, and G6 7.92 ppm) (Table II) and the X·A 9-mer duplex at basic pH (G4 7.80 ppm, X5 7.61 ppm, and G6 7.92 ppm) (Kouchakdjian et al., 1990) suggest that the upfield chemical shift values at G4 and X5 relative to G6 reflect better stacking between G4 and X5 than between X5 and G6 in both duplexes.

The H6 (7.78 ppm) and H5 (6.06 ppm) protons of C15 in the X·F 9-mer duplex (Table II) and the corresponding protons in the A·F 9-mer duplex (Kalnik et al., 1988a) are shifted downfield relative to their positions in stacked duplexes. This reflects the absence of a base at F14, resulting in the loss of base–base stacking interactions at F14–C15. The downfield shift of the H1′ proton of C13 (5.97 ppm) in the X·F 9-mer duplex (Table II) was also observed for the H1′ proton of C13 (5.61 ppm) in the A·F 9-mer duplex (Kalnik et al., 1988a) but to a lesser degree.

The observation of several phosphorus resonances to low and high field of the −4.0 to −4.5 ppm range in the phosphorus spectrum of the X·F 9-mer duplex (Figure 1C) suggests perturbation of the phosphodiester backbone (Connolly & Eckstein, 1984; Roongta et al., 1990) in this modified DNA helix. The shifted phosphorus resonances remain unassigned at this time. It should be pointed out that downfield-shifted phosphorus resonances have been detected and assigned for cyclic abasic sites positioned opposite dA (Kalnik et al., 1989a) and both downfield- and upfield-shifted phosphorus resonances have been detected for 1,N^2-propanodeoxyguanosine positioned opposite *dA* (Kouchakdjian et al., 1990).

Structural Conclusions. The NOESY data on the X·F 9-mer duplex readily establish that X5 is directed into the DNA helix and that the cyclic abasic site F14 is part of a regular sugar–phosphate backbone and is not looped out of the helix. We have used a single starting model and included only energy minimization in our computational studies. Thus, the minimized structure is simply one that meets the distance bounds and is in a local energy minimum. The major structural conclusion is that the exocyclic ring of the 1,N^2-propanodeoxyguanosine adduct fits into the cavity generated by the abasic site without disruption of the flanking G·C pairs.

Summary. Base pairing stabilized by hydrogen bonding is the central feature of the Watson–Crick DNA double helix. The hydrogen-bonding edge can be modified as a result of exocyclic adduct formation or where the base is deleted to form abasic sites. These lesions result in alignments stabilized in some cases by altered hydrogen-bonding arrangements. Our research, which involves a variety of DNA lesions, emphasizes the interplay between hydrogen-bonding and hydrophobic stacking interactions centered about the lesion site and the modulation of these interactions by pH (Kouchakdjian et al., 1989, 1990).

Previous studies established the deoxyadenosine stacks into rather than looping out of the helix when positioned opposite cyclic (Cuniasse et al., 1987; Kalnik et al., 1988a) and acyclic (Kalnik et al, 1989a) abasic sites. The present study extends our earlier observations by demonstrating that 1,N^2-propanodeoxyguanosine exocyclic adduct also stacks into the helix when positioned opposite a cyclic abasic site. In a sense, the 1,N^2-propanodeoxyguanosine and the tetrahydrofuran abasic site are complementary in that the additional ring of the exocyclic is accommodated by the cavity generated by the abasic site. The two lesions align without hydrogen bond formation and are stabilized by stacking of the 1,N^2-propanodeoxyguanosine adduct in the anti conformation between Watson–Crick G·C pairs in the X·F 9-mer duplex **3**. The X5·F14 dual lesion is accommodated without disruption of the flanking G4·C15 and G6·C13 pairs as reflected in the NOE and chemical shift parameters monitored at flanking base pairs.

Acknowledgments

We thank Prof. David Live of Emory University for recording the heteronuclear phosphorus–proton COSY experiment on the X·F 9-mer duplex whose contour plot is presented in Figure S3, supplementary material. NMR studies were conducted on instruments purchased with funds provided by the Robert Woods Johnson, Jr., Charitable Trust and Matheson Foundation.

Supplementary Material Available

Figures showing a one-dimensional NOE difference spectrum of the X·F 9-mer duplex in H_2O buffer, pH 7.3 at 10 °C (Figure S1), stacked plots of 250- and 50-ms NOESY contour plots of the base proton to H1′ proton region of the X·F 9-mer duplex in D_2O buffer, pH 7.3 at 10 °C (Figure S2), and a contour plot of the proton-detected proton–phosphorus heteronuclear COSY experiment on the X·F 9-mer duplex in D_2O buffer, pH 7.3 at 10 °C (Figure S3) (4 pages). Ordering information is given on any current masthead page.

Registry No. **2**, 132236-17-0; **3**, 132296-79-8.

References

Basu, A. K., & Essigmann, J. M (1988) *Chem. Res. Toxicol. 1*, 1–18.

Chung, F. L., Young, R. & Hecht, S. S. (1984) *Cancer Res. 44*, 990–995.

Connolly, B. A., & Eckstein, F. (1984) *Biochemistry 23*, 5523–5527.

Cuniasse, P., Sowers, L. C., Eritja, R., Kaplan, B., Goodman, M. F., Cognet, J. A., LeBret, M., Guschlbauer, W., & Fazakerley, G. V. (1987) *Nucleic Acids Res. 15*, 8003–8022.

Cuniasse, P., Sowers, L. C., Eritja, R., Kaplan, B., Goodman, M. F., Cognet, J. A., LeBret, M., Guschlbauer, W., & Fazakerley, G. V (1989) *Biochemistry 28*, 2018–2026.

Cuniasse, P., Fazakerley, G. V., Guschlbauer, W., Kaplan, B. E., & Sowers, L. C. (1990) *J. Mol. Biol. 213*, 303–314.
Hare, D., Wemmer, D. E., Chou, S. H., Drobny, G., & Reid, B. R. (1983) *J. Mol. Biol. 171*, 319–336.
Harris, T. M., Stone, M. P., & Harris, C. M. (1988) *Chem. Res. Toxicol. 1*, 79–96.
Kalnik, M. W., Chang, C.-N., Grollman, A. P., & Patel, D. J. (1988a) *Biochemistry 27*, 924–931.
Kalnik, M. W., Kouchakdjian, M., Li, B. F., Swann, P. F., & Patel, D. J. (1988b) *Biochemistry 27*, 100–108.
Kalnik, M. W., Kouchakdjian, M., Li, B. F., Swann, P. F., & Patel, D. J. (1988c) *Biochemistry 27*, 108–115.
Kalnik, M. W., Chang, C.-N., Johnson, F., Grollman, A. P., & Patel, D. J. (1989a) *Biochemistry 28*, 3373–3383.
Kalnik, M. W., Li, B. F., Swann, P. F., & Patel, D. J. (1989b) *Biochemistry 28*, 6170–6181.
Kalnik, M. W., Li, B. F., Swann, P. F., & Patel, D. J. (1989c) *Biochemistry 28*, 6182–6192.
Kouchakdjian, M., Marinelli, E., Gao, X., Johnson, F., Grollman, A., & Patel, D. J. (1989) *Biochemistry 28*, 5647–5657.
Kouchakdjian, M., Eisenberg, M., Live, D., Marinelli, E., Grollman, A. P., & Patel, D. J. (1990) *Biochemistry 29*, 4456–4465.
Lindahl, T. (1982) *Annu. Rev. Biochem. 51*, 61–87.
Lindahl, T., & Nyberg, B. (1972) *Biochemistry 11*, 3610–3618.
Loeb, L. (1985) *Cell 40*, 483–484.
Marinelli, E. R., Johnson, F., Iden, C. R., & Yu, P. L. (1990) *Chem. Res. Toxicol. 3*, 49–58.
Millican, T. A., Mock, G. A., Chauncy, M. A., Patel, T. P., Eaton, M. A., Gunning, J., Cutbush, S. D., Neidele, S., & Mann, J. (1984) *Nucleic Acids Res. 12*, 7435–7453.
Norman, D., Abuaf, P., Hingerty, B. E., Live, D., Grunberger, D., Broyde, S., & Patel, D. J. (1989) *Biochemistry 28*, 7462–7476.
Otting, G., Widmer, H., Wagner, G., & Wuthrich, K. (1986) *J. Magn. Reson. 66*, 187–193.
Patel, D. J., Kozlowski, S. A., Nordheim, A., & Rich, A. (1982) *Proc. Natl. Acad. Sci. U.S.A. 79*, 1413–1417.
Patel, D. J., Shapiro, L., Kozlowski, S. A., Gaffney, B. L., & Jones, R. A. (1986a) *Biochemistry 25*, 1027–1036.
Patel, D. J., Shapiro, L., Kozlowski, S. A., Gaffney, B. L., & Jones, R. A. (1986b) *Biochemistry 25*, 1036–1042.
Patel, D. J., Shapiro, L., Kozlowski, S. A., Gaffney, B. L., & Jones, R. A. (1986c) *J. Mol. Biol. 188*, 677–692.
Plateau, P., & Gueron, M. (1982) *J. Am. Chem. Soc. 104*, 7310–7311.
Pochet, S., Huynh-Dinh, T., Neumann, J. M., Tran-Dinh, S., Adam, S., Taboury, J., Taillandier, E., & Igolen, J. (1986) *Nucleic Acids Res. 14*, 1107–1126.
Raap, J., Dreef, C. E., van der Marel, G. A., van Boom, J. H., & Hilbers, C. W. (1987) *J. Biomol. Struct. Dyn. 5*, 219–247.
Roongta, V. A., Jones, C. R., & Gorenstein, D. G. (1990) *Biochemistry 29*, 5245–5258.
Schwartz, A., Marrot, L., & Leng, M. (1989) *J. Mol. Biol. 207*, 445–450.
Shapiro, R. (1969) *Ann. N.Y. Acad. Sci. 163*, 624–630.
Singer, B., & Grunberger, D. (1983) in *Molecular Biology of Mutagens and Carcinogens*, Plenum Press, New York.
Singer, B., & Bartsch, H. (1986) *The Role of Cyclic Nucleic Acid Adducts in Carcinogenesis and Mutagenesis*, IARC Scientific Publications 70, International Agency for Research on Cancer, Lyon, France.
Takeshita, M., Chang, C.-N., Johnson, F., Will, S., & Grollman, A. P. (1987) *J. Biol. Chem. 262*, 10171–10179.
Vesnaver, G., Chang, C. N., Eisenberg, M., Grollman, A. P., & Breslauer, K. J. (1989) *Proc. Natl. Acad. Sci. U.S.A. 86*, 3614–3618.
Weiss, B., & Grossman, L. (1987) *Adv. Enzymol. Relat. Areas Mol. Biol. 60*, 1–34.